ISSN 1345-3041

Sep.2015 / Vol.151

Mitsubishi Electric

ADVANCE

Aiming to Achieve a Higher Level of Environmental Management

MITSUBISHI ELECTRIC
Changes for the Better

Sep. 2015 / Vol. 151

Mitsubishi Electric ADVANCE

Aiming to Achieve a Higher Level of Environmental Management

• **Editorial Inquiries**
Kiyoshi Sakai
Corporate Total Productivity Management & Environmental Programs
Fax: +81-3-3218-2465

• **Product Inquiries**
Motohiro Tanaka
Corporate Environmental Sustainability Group
Fax: +81-3-3218-2465

Mitsubishi Electric ADVANCE is published on line quarterly (in March, June, September, and December) by Mitsubishi Electric Corporation.

CONTENTS

Technical Reports

Precis

While continuing to meet the social demand for safe and convenient lifestyles, Mitsubishi Electric aims to help create a sustainable global environment through a wide variety of products in all aspects of society, advanced technologies, and optimized systems. Here we show some of our latest businesses and technologies geared toward a low-carbon, recycling-based society.

Overview

Author: *Tomohiko Nambara**

Environmental issues used to be related to mainly environmental destruction directly resulting from manufacturers' production activities, such as environmental pollution issues, but many of these problems have substantially been brought under control of the society since the beginning of the 21st century.

Thus, society's expectations for companies are shifting to the environmental contributions of their business activities, that is, the contributions of their products, services and technologies to environmental improvement and conservation.

For instance, to create a low-carbon society to help mitigate climate change, it is essential to reduce the use of energy in human activities and hence fossil fuel consumption. Compared with the energy used during production, energy consumed during the usage of products accounts for a greater proportion. Therefore, Mitsubishi Electric must improve the energy performance of its products and services. This special edition includes examples of the latest technologies: silicon carbide (SiC) power semiconductors, high-efficiency heat pump systems, and grid connection technologies for effectively using renewable energy resources.

To create a recycling-based society, in addition to reducing the amount of landfill waste resulting from production, it is increasingly more important for the products, technologies, and business activities themselves should also contribute to the recycling of materials. Mitsubishi Electric has developed and commercialized advanced technologies for recycling plastics from post-consumer electric home appliances, as well as an environment-friendly ozone water purification system, both of which are presented in this special edition.

Mitsubishi Electric will continue to help create a better, safer society by conserving the environment, striving for growth with high quality to be a "Global, Leading Green Company" acknowledged by society.

**Group President, Corporate Environmental Sustainability Group*

Energy Saving Driven by SiC Power Semiconductors

Author: *Katsumi Sato** and *Junji Yamada**

1. Introduction

Mitsubishi Electric has a long history in the development of silicon carbide (SiC) devices, starting with basic product development in the 1990s, verification and demonstration tests in the 2000s, and the shipment of samples in 2010 for potential mass production. Some products that are already being mass produced contribute to the energy saving, downsizing and weight saving of power electronics (PE) equipments.

This paper describes the present status of Mitsubishi Electric SiC modules and their applications.

2. SiC Chips

2.1 Development status of SiC chips

A 600 V Schottky barrier diode (SBD) was the first SiC device marketed by Mitsubishi Electric. We have integrated SiC-specific processes and Mitsubishi Electric's established know-how in the semiconductor field to develop a process flow that satisfies the quality requirements. The SiC-SBD chips are assembled in various hybrid SiC module types. The feedback from their evaluation results helped to improve product characteristics and quality. At present, we have an SBD product line with rated blocking voltage ranging from 600 to 3300 V and a rated current of up to 150 A.

It is difficult to fabricate a large-area SiC-SBD with the design because of defects present in the SiC wafer and epitaxial layer. Therefore, in contrast to Si diodes that have a rated current of up to 300 A, the SiC-SBD has a relatively low rated current. Mitsubishi Electric is continuously improving the quality of the wafer and epitaxial layer, aiming to achieve a rated current equivalent to that of the Si diode.

Mitsubishi Electric has also developed an SiC metal-oxide-semiconductor field-effect transistor (MOSFET) in a planar gate structure, and released a product line with rated voltage of 600 V, 1200 V and 3300 V. The maximum rated current is 300 A (1200 V), and efforts to enhance the rated current are in progress similarly to the SBD.

Figure 1 shows an external view and the on-state characteristics of a 300 A MOSFET with a rated voltage of 1200 V. The current and temperature sensing functions are embedded in an effective area of 1 cm^2.

The on-state resistance at 150°C has been reduced to 8.6 mΩ. As shown in the turn-off waveform depicted in Fig. 2, in comparison with the Si-insulated-gate bipolar transistor (IGBT), the SiC-MOSFET has a smaller tail current in the turn-off operation. In addition, the reverse-bias safety operating area (RBSOA) test have proven the SiC-MOSFET's turn-off capability of 2500 A/cm^2, confirming its robustness as an advantage over the unipolar device.

2.2 Technical development trend

Following the 1200 V SBD and MOSFET, we are developing a high-voltage device series. In a comparison between the 1200 V and 3300 V MOSFETs, the rated blocking voltage is almost proportional to the

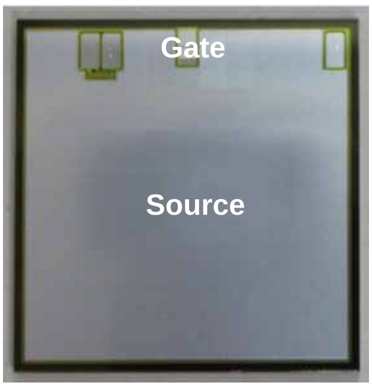

(a) SiC-MOSFET

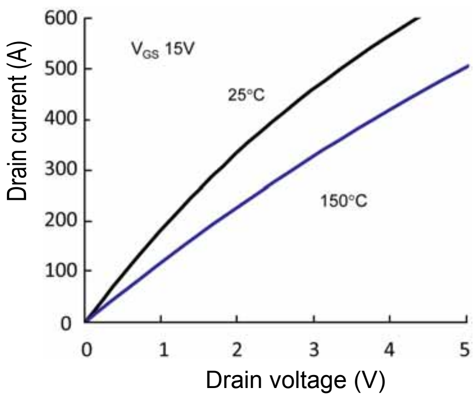

(b) On-state characteristics

Fig. 1 External view and on-state characteristics of SiC-MOSFET with isolation voltage of 1200 V and effective area of 1 cm^2

**Power Device Works*

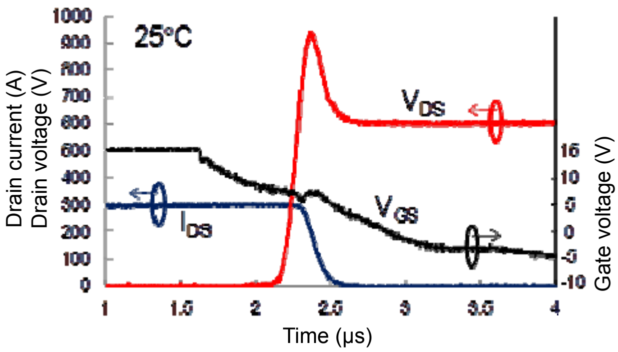

Fig. 2 Turn-off switching waveform of SiC-MOSFET with isolation voltage of 1200 V and effective area of 1 cm^2

thickness and resistivity of the epitaxial layer. Since the on-state resistance of a high-voltage device is influenced by the resistivity of the epitaxial layer, the on-state resistivity of the 3300 V MOSFET generally becomes nearly 10 times that of the 1200 V MOSFET. Thus, an important issue for a high-voltage device is to reduce the on-state resistance. For the 3300 V MOSFET, we took various ideas such as n-type ion implantation in the region of the junction field-effect transistor (JFET) to reduce the JFET resistance. Consequently, we have successfully reduced the on-state resistance to 39 mΩcm^2 at 150°C, which is less than five times that of the 1200 V MOSFET, or almost one-half that without any ideas taken. Figure 3 shows the cross-sectional schematics, and on- and off-state characteristics of the 3300 V MOSFET currently under development.

Usually, the parasitic body diode of a high-voltage MOSFET should not be used as a freewheeling diode (FWD) because of the degradation of its on-state performance through operation. To enable FWD application with the Mitsubishi Electric 3300 V SiC-MOSFET, a high-quality epitaxial layer is being developed for more compact and lighter modules.

In addition to enlarging the rated voltage, a trench gate type MOSFET is also being developed to further reduce the resistance. The trench gate structure can eliminate the JFET resistance that is unavoidable with the planar gate structure. We plan to use this structure for MOSFETs of low to medium voltage, i.e., 600 to 1200 V, in which the JFET resistance accounts for a major part of the on-state resistance.

3. SiC Module

3.1 Present product line of SiC modules

Mitsubishi Electric has released the SiC product line including: 1700 V/1200 A hybrid SiC module for railways; 1200 V/1200 A full SiC module for elevators; 75 A/1200 V 6 in 1 full SiC intelligent power module (IPM) for motor control; and hybrid dual inline package

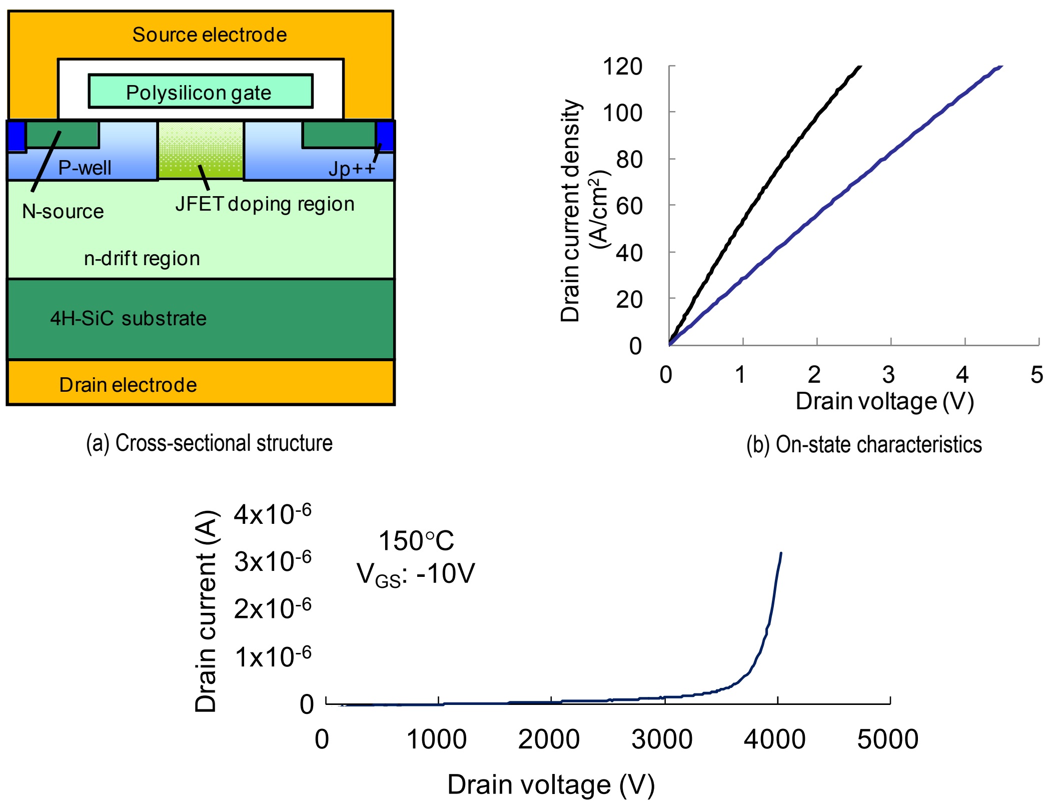

(a) Cross-sectional structure

(b) On-state characteristics

(c) Off-state characteristics

Fig. 3 Cross-sectional schematics and on- and off-state characteristics of SiC-MOSFET with isolation voltage of 3.3 kV

IPM (DIPIPM) for air conditioners, thus reducing the power consumption, size, and weight of equipment. An advantage of the SiC modules offered by Mitsubishi Electric is the flexible combination of the SiC-MOSFET, SiC-SBD, Si-IGBT, fast-switching IGBT, and other devices to develop an application-specific, cost-effective module product.

3.2 Hybrid SiC module

The hybrid SiC module consists of a combination of Si-IGBTs and SiC-SBDs, and can be used in the same manner as the conventional IGBT module. The hybrid SiC module has the advantage of lower FWD reverse-recovery loss and lower IGBT turn-on switching loss compared to the conventional IGBT module.

We are currently developing hybrid SiC modules for the Mitsubishi Electric “NFH Series,” a high-frequency product line for industrial applications, with the same current and voltage ratings and in the same package as those of the conventional IGBT modules. The compatible design allows present NFH users to adopt the hybrid SiC modules without any modification of the present busbar layout or peripheral circuits. If the hybrid SiC module is used under the same conditions as that of the present IGBT module, the total power loss can be significantly reduced, e.g., by about 50% at a switching frequency of 30 kHz (Fig. 4). The reduction in power loss makes it possible to reduce the number of cooling fins and fans, and in turn allows a compact and lighter enclosure design. As another possibility, the operating frequency can be increased with the same heat dissipation system, e.g., the IGBT total power loss at a switching frequency of 17 kHz is nearly the same as that of the hybrid SiC module at 50 kHz (Fig. 4), and this higher frequency enables the coils and other inductors in the circuit to be made smaller.

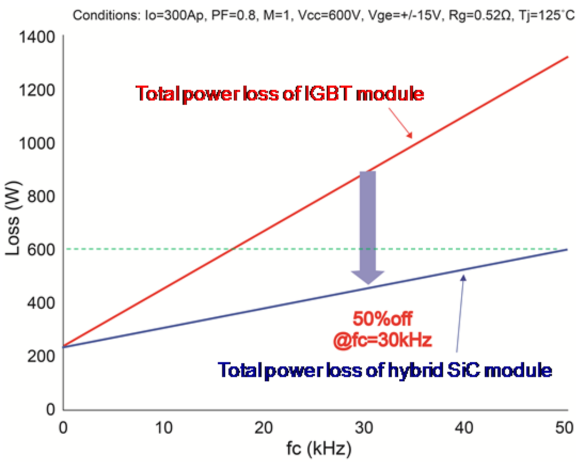

Fig. 4 Total power loss of modules vs. switching frequency

3.3 Full SiC module

The full SiC module consists of a combination of SiC-MOSFETs and SiC-SBDs, or SiC-MOSFETs only. Mitsubishi Electric currently offers product lines of standard-type full SiC modules and full SiC IPMs that integrate a drive circuit, a protection circuit, etc. By using a MOSFET unipolar device, the loss is reduced to at least half that of the hybrid SiC module.

Most conventional SiC MOSFETs have a threshold gate voltage lower than that of the Si-IGBT and a high gate drive voltage, and thus suffer from the drawback of needing a special gate drive circuit or having a small noise margin against malfunction. To facilitate replacement of conventional IGBT modules, Mitsubishi Electric has designed the full SiC modules to allow the continued use of drivers with the same drive voltage (15 V) as that of the conventional IGBTs.

4. Application Examples of SiC Modules

4.1 Hybrid SiC module for railway application

Mitsubishi Electric not only has a large market share of the IGBT modules mounted on traction inverters for railway vehicles, but is also in a leading position in the development and mass production of the SiC modules. The world’s first SiC module for railway vehicle application[1] is the dual 1700 V/1200 A hybrid SiC module (Fig. 5), which is mounted on an SiC module traction inverter. It was produced at Mitsubishi Electric Itami Works in October 2011. The use of SiC chips for the inverter successfully reduced power loss by 30% and volume and mass by 40% from the level of conventional equipment. The next SiC module developed for railway application is a dual 3300 V/1500 A full SiC module. It is mounted on a variable-voltage variable-frequency (VVVF) inverter system corresponding to the DC1500 V catenary voltage, and is presently undergoing an actual running test. The new system has not only reduced the equipment power loss by about 55% from the conventional level, but has also reduced the energy consumption of the entire rolling stock, including the traction motors, by approximately 30%. In addition, the volume and mass are both reduced by approximately 65%.

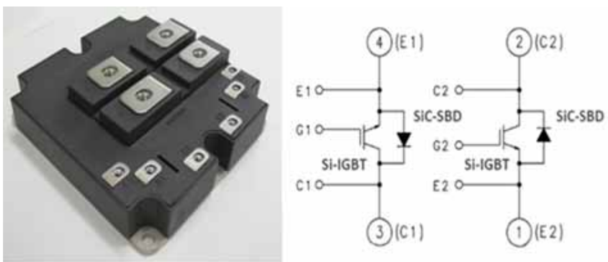

Fig. 5 Dual 1700 V/1200 A hybrid SiC module for railway vehicle application

1 Internal research by Mitsubishi Electric as of October 3, 2011.

4.2 Full SiC module for elevator application

SiC modules are increasingly being used in elevator control systems, which is an industrial application that requires high reliability. In most cases, the elevator control system is installed together with the motor in a machine room located at the top of the building. Due to space constraints, the machine room must be smaller and lighter. Energy saving is also important. To solve these issues, for the first time in the industry, the dual 1200 V/1200 A full SiC module with the world's largest rated current [2] was adopted for the controller of Mitsubishi Electric's high-speed elevator system (Fig. 6). Demonstration tests on the elevator system are currently under way prior to mass production. In this application, the full SiC module has reduced the power semiconductor loss by approximately 65%, and the high-frequency switching has allowed smaller reactors in the power supply, reducing the controller volume and footprint by approximately 40%.

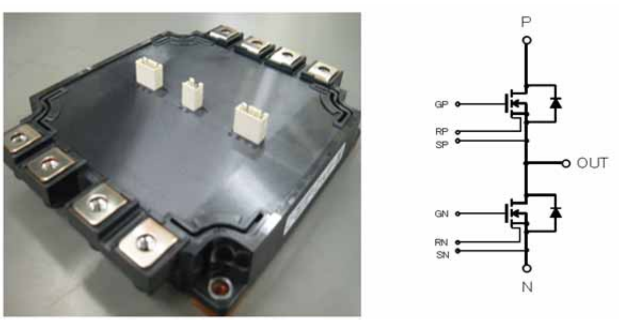

Fig. 6 Dual 1200 V/1200 A full SiC module for high-reliability industrial application

5. Issues with SiC Modules and Future Applications

In comparison with Si-based devices, SiC devices offer lower power loss with higher rated blocking voltage, higher temperature operation, higher switching speed, and lower thermal resistance. With these advantages, SiC devices are expected to be used for various applications in the future. Some applications are already in progress including: power transmission and railway applications utilizing their high rated blocking voltage and low power loss; medical power supplies relying on high-speed switching capability; and solar power converters.

Meanwhile, to make full use of the high-temperature operation, the packaging technology needs to be improved to handle the higher chip temperature. In this field, too, Mitsubishi Electric will develop advanced technologies to keep up with the increasing chip temperature. Some basic technologies have already been put into mass production, and will be used in the next-generation SiC module.

2 Internal research by Mitsubishi Electric as of February 2013.

6. Conclusion

Mitsubishi Electric will integrate its wafer technology and packaging technology established through years of experience to enhance the SiC module performance, and thus help create a sustainable and low-carbon society through the energy saving of power electronics.

This work has been partially supported by Japan's New Energy and Industrial Technology Development Organization(NEDO).

Technologies for Connecting Renewable Energy Resources to the Electricity Grid

Author: *Yasuhiro Kojima** and *Tomihiro Takano***

1. Introduction

As a power source for a low-carbon society and for ensuring energy security in Japan, photovoltaic (PV), wind turbine (WT) and other renewable energy systems are increasingly being interconnected with the electricity grid. However, this is causing concern about the deterioration of power quality due to susceptibility to weather and large fluctuations in renewable power generation. Figure 1 summarizes the issues related to the introduction of renewable energy.

This paper describes the supply and demand control system and distribution voltage control system, which stabilize the frequency and distribution line voltage corresponding to the increasing number of renewable energy sources. The supply and demand control system balances the supply and demand on the whole grid to keep a constant frequency on the power network. The distribution voltage control system balances the local generation and consumption of electricity to keep a constant line voltage. The operation of each system has already been verified at our in-house demonstration test facilities, and some of these systems have already been implemented in an actual grid.

2. Supply and Demand Control System

2.1 System overview

In response to the variation in demand, the supply and demand control system adjusts the number of generators in operation and the amount of generation in thermal, pumped storage, and other controllable power stations, thus balancing the supply and demand to keep the frequency within an appropriate range. To achieve this control, the supply and demand control system mainly consists of a demand forecast function, a supply-demand planning function, and a supply-demand control function. The demand forecast function estimates the demand on the next day based on past climate data and regional characteristics using regression analysis models, etc. Based on this forecast, the supply-demand planning function determines the

Item	Image	Phenomena and issues
Fluctuation	Example of PV output fluctuation 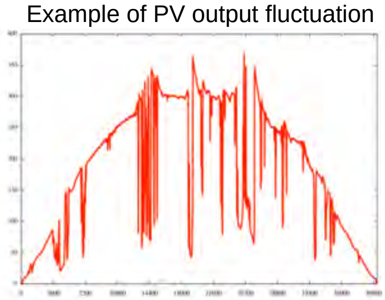	Output power is dependent on the weather, and difficult to control Supply-demand imbalance occurs Frequency fluctuation
Excess/ Shortage	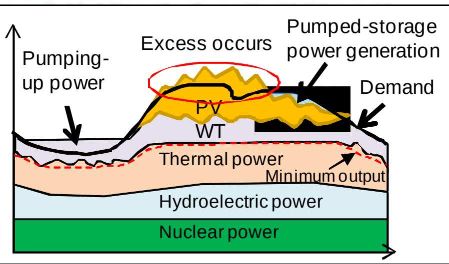	High PV output when the load is light Inaccurate forecasting of power generation Excess PV power Supply capacity shortage when the forecast is inaccurate
Voltage	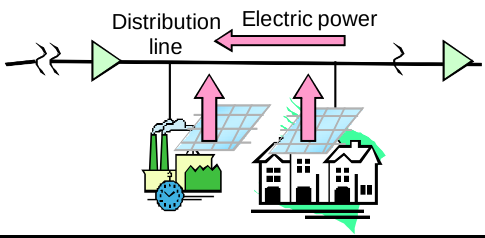	Electric power flows back from consumers to the grid Fluctuation in the distribution line voltage Upper voltage limit is exceeded

Fig. 1 Issues related to the introduction of renewable energy

*Transmission & Distribution Systems Center   **Advanced Technology R&D Center start or stop timing of the generators for the day, and the supply-demand control function performs real-time control in response to the constantly fluctuating demand.

However, if the grid is interconnected with a large number of PV and WT resources providing unstable generation output, forecasting and monitoring is required not only for the power demand but also for the PV and WT generation output, and the supply-demand control must be prepared for fluctuations. In addition, a variable-speed pumped-storage generator, grid storage battery, and other large-scale energy storage systems are being developed to compensate for the variation in PV and WT generation output. Consequently, for the full utilization of PV and WT power generation, an advanced supply-demand control system is required to coordinate the power generators that used to be the only control object, as well as the new energy storage systems, and users. The next section describes the technologies for coping with a large number of renewable energy resources, to be introduced by controlling the supply and demand through the adoption of storage batteries.(1)

2.2 Grid stabilization control using storage battery system

The variability of renewable energy poses two problems: an instantaneous short-period problem and a day-long, long-period problem. To deal with uncertain supply and demand imbalances, the storage battery system is a promising replacement for the pumped-storage generator because of the ease of finding a candidate site and the short lead time from start of construction to start of operation, although the cost of the battery itself needs to be reduced. Promising battery types with suitable characteristics are lithium for the short-period problem and NAS[1] for the long-period problem.

To ensure the power quality on a small-scale grid, e.g., on an isolated island, in addition to the conventional ΔF control, we have developed the new ΔP control method for the active power of storage batteries. While the ΔF control detects variations in the frequency, the new ΔP control detects variations in the power flowing through the interconnected line. Each control method is outlined below.

(1) ΔF control

This conventional technique is a feedback control corresponding to deviations from the reference frequency that are caused by an imbalance between supply and demand. It has the advantage of working properly under any circumstances, but the control begins only after the frequency deviation occurs and thus operation is slower compared to the ΔP control, as described below.

(2) ΔP control

On an isolated island where the electric power is supplied by internal combustion generators and renewable energy resources are interconnected with the grid, the generator output is affected by variations in the output of renewable energy. Since the fuel supply to the generator cannot be changed immediately, an imbalance occurs between the mechanical input and the electric output in the internal combustion generator. This imbalance in turn changes the rotating speed and hence causes a frequency variation. The ΔP control method directly detects this imbalance by measuring the power flowing through the power line from the generator, and any short-period variations are compensated by the storage battery.

2.3 Results of demonstration test

This section describes the demonstration test results for the grid stability control system. In response to the promotion of renewable energy resources on isolated islands, Kyushu Electric Power Company has introduced a storage battery system at the Ashibe substation (Iki Island, Nagasaki prefecture), supported by a subsidy project of the Ministry of Economy, Trade and Industry, "FY2012 demonstration project for the promotion of wind power resources interconnected to the electricity grid."(2) The electricity grid on Iki Island is separated from the mainland and has a capacity of about 35,000 kW, which is supplied by two internal combustion power stations. As of March 2013, the frequency control capability had already reached its limit because of the WT energy resources interconnected with the grid. The introduced storage battery system is configured with eight storage battery units, each consisting of a 500-kW power conditioning system (PCS) and a 200-kWh lithium-ion battery (4000 kW, 1600 kWh) (Fig. 2).

In addition to the ΔF method and ΔP method for the grid stability control, ΔF + ΔP control, newly developed in collaboration with Kyushu EPCO, was also demonstrated (Fig. 3). In the demonstration tests conducted since FY2012, the ΔF + ΔP control has proven to reduce fluctuations not only in the power flowing through the interconnection line but also in the output of the internal combustion power generators. These results have confirmed the effectiveness of the storage battery system (Fig. 4).

3. Distribution Voltage Control System

3.1 System overview

When a large number of PV and other distributed power sources are interconnected with a distribution grid, the voltage could increase due to current backflow, or fluctuate due to changing weather. To solve these voltage problems, we have developed a dual-level distribution voltage control system, which combines a

[1] NAS is a registered trademark of NGK Insulators, Ltd.

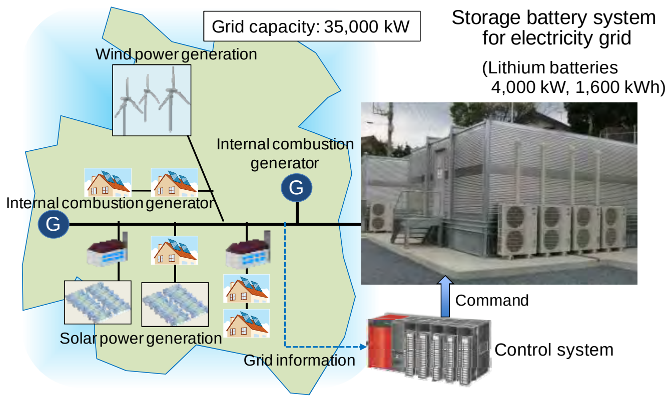

Fig. 2 Storage battery system for isolated island (solution for short-period fluctuations)

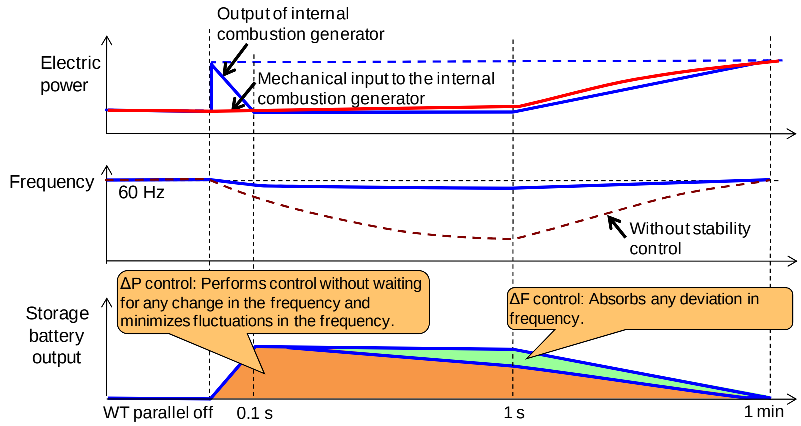

Fig. 3 Overview of ΔF + ΔP control

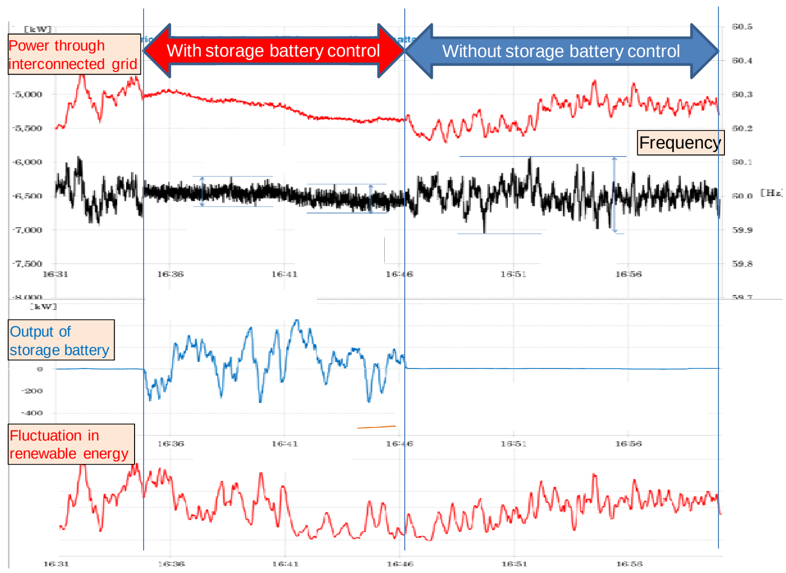

Fig. 4 One result of the demonstration test at an isolated island

centralized and a local control system (Fig. 5).

In this system, current and voltage measurements are acquired via a communication network from each switchgear equipped with a sensor installed in the power distribution system, and the optimal control command is determined for each control target using the Optimal Power Flow (OPF) calculation software installed in the automated power distribution system.[3]

Communication between the automated power distribution system and each device takes minutes because of the data processing and routing through multiple networks with an enormous amount of communication traffic. Meanwhile, the voltage fluctuation resulting from the fluctuation in PV output takes place in seconds. Therefore, with the centralized control system alone, where the automated power

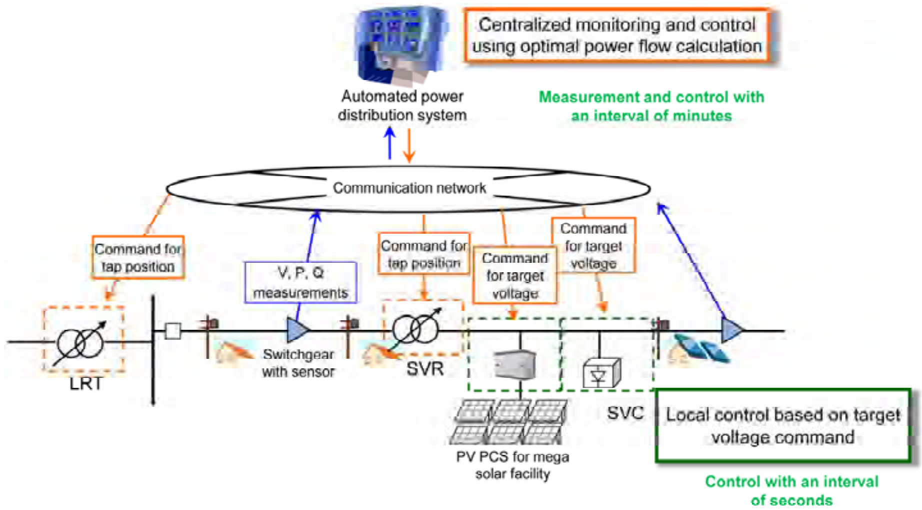

Fig. 5 Framework of dual-level distribution voltage control system

distribution system sends a command directly to each power distribution device, fluctuations in the voltage may not be stabilized. Consequently, we have combined the overall optimization by the centralized control system and the high-speed local control over the power electronics equipment to develop the dual-level control system.

3.2 Dual-level control system

The distribution voltage control devices are largely divided into the following two types:

(1) Mechanical tap switching type voltage regulator (Discrete control type)

The load-ratio control transformer (LRT) at the distribution substation and the step voltage regulator (SVR) on the distribution line are of this type. These are kinds of transformers, and the secondary voltage is raised or lowered by controlling taps to change the winding ratio.

(2) Reactive power control type power electronics voltage regulator (Continuous control type)

The static VAR compensator (SVC) on the distribution line and the PCS for industrial PV (PV-SVC) are included in this category. These devices raise or lower the voltage by adding or taking reactive power to or from the distribution line.

For Type (1), the power loss is small, but because of the mechanical structure, the number of control operations is limited to about 20 a day maximum. For Type (2), the power loss is larger than for Type (1), but the response speed is high. Based on these features, the target of dual-level control was set as: minimizing the power loss and properly maintaining the voltage by absorbing instantaneous short-period fluctuations in voltage by controlling Type (2) devices, and dealing with medium- and long-period variations in voltage by the centralized control of Type (1) devices. To this end, the object functions for the OPF were defined as the following three elements: (a) voltage deviation, (b) number of tap operations, and (c) power loss resulting from the reactive power control, with a weighting relationship of (a) >> (b) ≥ (c).

To control Type (1) devices with a period of minutes, the OPF calculation is performed based on the measurements (V: voltage, P: active power, Q: reactive power) acquired at each measuring point on the distribution line, and the optimal combination of Type (1) and (2) control is determined for minimizing the object functions, and then the resulting voltage distribution (post-control voltage distribution) is determined by the power flow calculation. The Type (1) control value determined (tap position) is sent out as a direct command to each LRT or SVR. In parallel, for Type (2) devices, the voltage in the post-control voltage distribution at each device location is provided as the target voltage. For the local control of each Type (2) device, the reactive power is controlled by the proportional integral (PI) control with a period of one second, so the deviation between the present grid voltage and the given target voltage is reduced. Therefore, if there is no fluctuation in the grid voltage, each Type (2) device provides the constant reactive power output determined by the OPF. In reality, however, voltage fluctuation occurs before the next OPF control period, and to maintain the voltage distribution determined by the OPF, the reactive power output is varied as required.

3.3 Results of demonstration test

We evaluated the validity of the developed system using the smart grid demonstration test facility at the Mitsubishi Electric Amagasaki site. Figure 6 shows the distribution grid at this facility. A substation equipped with an LRT is shown at the upper left corner of the diagram. The system is configured to simulate an electricity grid having a large voltage difference between the end points

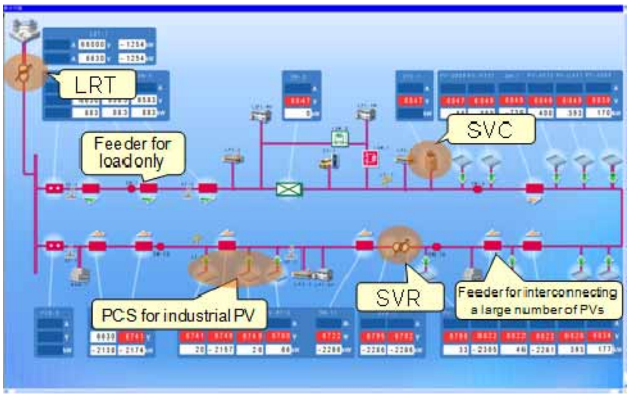

Fig. 6 Distribution grid diagram at Amagasaki site

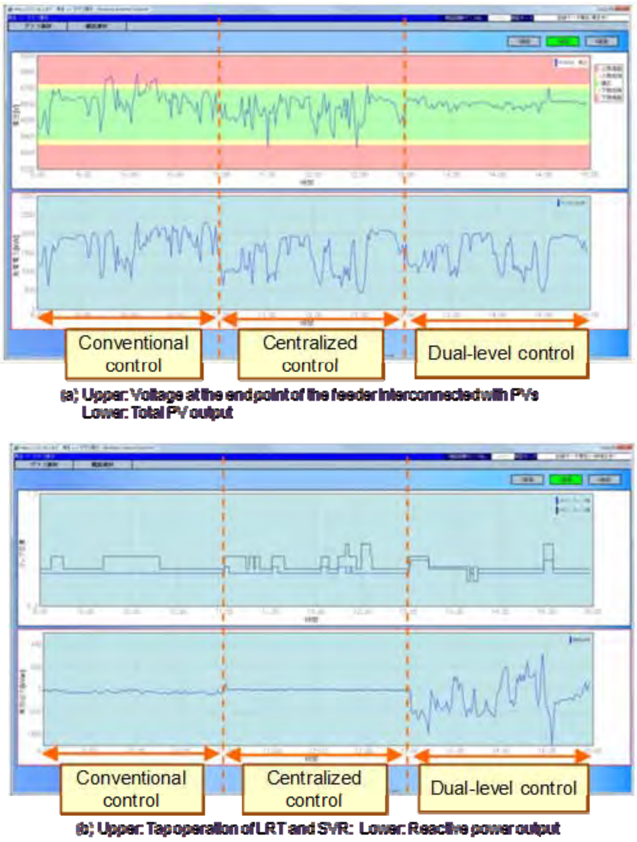

Fig. 7 Demonstration test results for distribution voltage control

of two feeders: a feeder for load only (the line up to the upper boundary point in the diagram), and a longer feeder, 10 km in length, for interconnecting a large number of 3-MW PVs (the line going around the lower side and up to the upper boundary point). The feeder interconnected with many PVs is equipped with an LRT as a voltage regulator installed at the substation, an SVR at the midpoint of the feeder, an SVC at the end point, and distributed industrial PV PCSs. In the demonstration test, the following three control methods were evaluated and compared:

(1) Conventional control: Local control using LRT and SVR
(2) Centralized control: Centralized control over LRT and SVR
(3) Dual-level control: Dual-level control for LRT, SVR, SVC and PV PCS

Figure 7 shows the results of 2-h demonstration tests conducted for the conventional control, centralized control and dual-level control in that order. The upper chart in Fig. 7 shows the grid voltage at the end point of the feeder interconnected with many PVs, which exhibits the largest increase and fluctuations in voltage. The goal of the control is to keep the voltage within the appropriate range indicated at the center.

These results show that in comparison with the conventional control, the centralized control reduces the occurrence of exceeding the upper voltage limit, although the number of LRT and SVR tap operations increases. However, with this voltage control, large fluctuations in PV output cannot be stabilized, and small voltage deviations occur. In contrast, the dual-level control that utilizes the reactive power control by means of the SVC and PV PCS (total capacity of 450 kVar) completely eliminates the deviation in voltage and reduces the amplitude of the variations in voltage by about 70%. In addition, as shown by the upper chart in Fig. 7, in comparison with the centralized control, the number of LRT and SVR tap operations is also reduced.

The demonstration test has confirmed that the dual-level control can effectively reduce the deviation in voltage and the number of tap operations.

4. Conclusion

In response to the issues arising from the interconnection of renewable energy resources with the electricity grid, we have developed a solution based on supply and demand control and distribution voltage control. The demonstration test results provided the desired effects, and in terms of promoting renewable energy, we believe it is possible to stably control the power network, maintain a safe power supply, and help create a low-carbon society.

References

(1) Yasuhiro Kojima: Energy Management System for Smart Grid/Smart Community, Measurement and Control, 53, No. 1, 56–61 (2014) (in Japanese)
(2) Fumitoshi Nomiyama, et al.: Demonstration Test of Frequency Fluctuation Suppression Using a Storage Battery in Isolated Island System, AORC-CIGRE Technical Meeting (2014)
(3) Tetsufumi Ohno, et al.: Optimal Control Technology for Smart Grid Distribution System, Conference of the IEEJ Power and Energy Society General Meeting, 271 (2010) (in Japanese)

Contributing to the Air to Water Heat Pump Business by Developing an Energy Simulation Tool

Author: *Hiroshi Maitani**

Mitsubishi Electric is promoting air to water (ATW) space heating and hot water supply systems as renewable energy sources for domestic houses in Europe. We have developed an ATW energy simulation tool to enhance the ATW business. This tool simulates annual energy consumption, running cost, and CO_2 emissions, and is useful for optimizing a product to suit various conditions of the customer.

1. Introduction

The EU has decided to reduce greenhouse gas emissions (GRG) by 20% by 2020 compared with 1990 and so is encouraging the introduction of renewable energy sources. Figure 1 shows an example of the energy consumed by a typical European residential house. Hot water and space heating account for about 60% of the total energy consumption.

Traditionally, radiation heating using hot water is used for space heating, and a gas or oil boiler supplies heat to the heating equipment and hot water tank. Mitsubishi Electric aims to replace the boiler by air to water (ATW) as shown in Fig. 2 using heat pump technology with high efficiency and low CO_2 emissions, because the EU has designated the heat pump as a renewable energy source and some countries have introduced incentive schemes. We describe our ATW energy simulation tool to support the ATW business in Europe.

2. Climatic Variations in Europe

Figure 3 shows the different climate zones in Northern, Central and Southern Europe, as the performance of a heat pump is strongly affected by climate. In addition, the energy source used for space heating differs greatly in each country. Figure 4 shows

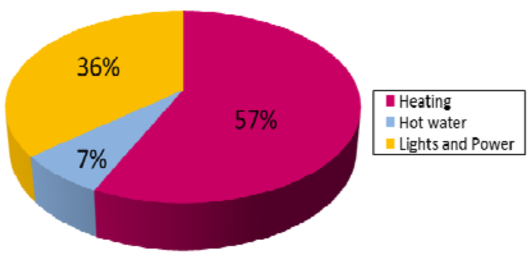

Fig. 1 Breakdown of energy consumption in domestic house(1)

Fig. 3 Climate zones in Europe(2)

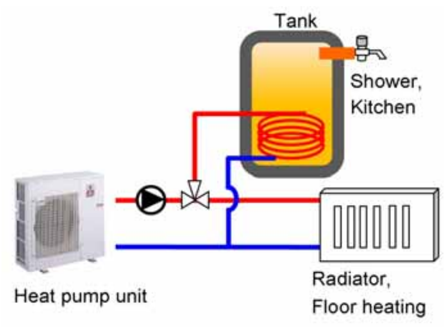

Fig. 2 Air to water system

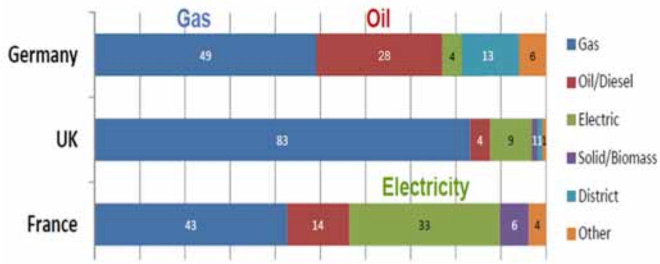

Fig. 4 Energy source for space heating(4)(5)(6)

*Mitsubishi Electric R & D Centre Europe B.V.

the features of the energy sources used in each country. Natural gas is mainly used in the UK, while electricity generated by nuclear power is mainly used in France. Hence, the energy cost and CO_2 emissions for hot water supply and space heating vary among countries, and so the business strategy must be tailored to each country to enhance the ATW business.

3. ATW Energy Simulation Tool

Mitsubishi Electric R&D Centre Europe B.V. (MERCE) developed the ATW energy simulation tool with Mitsubishi Electric Air Conditioning Systems Europe Ltd. (M-ACE), as outlined in Fig. 5. This version is for France but can also be used in other countries.

(1) Input conditions

Various conditions such as residential area, building insulation, type of heating equipment and heating operating conditions are input to calculate the heating load of the customer's house.

(2) Database

This tool has a climate database to calculate the heating load from the residential area, product and radiator performance database to calculate energy consumption, and energy database to calculate annual running cost and CO_2 emissions. The climate data and energy data are different for each country.

(3) Output

The simulation result shows the recommended product combination for a particular customer, which can easily be compared with other product combinations.

- Capacity at designed ambient temperature to check that enough heat can be supplied
- Annual running cost and CO_2 emissions to show

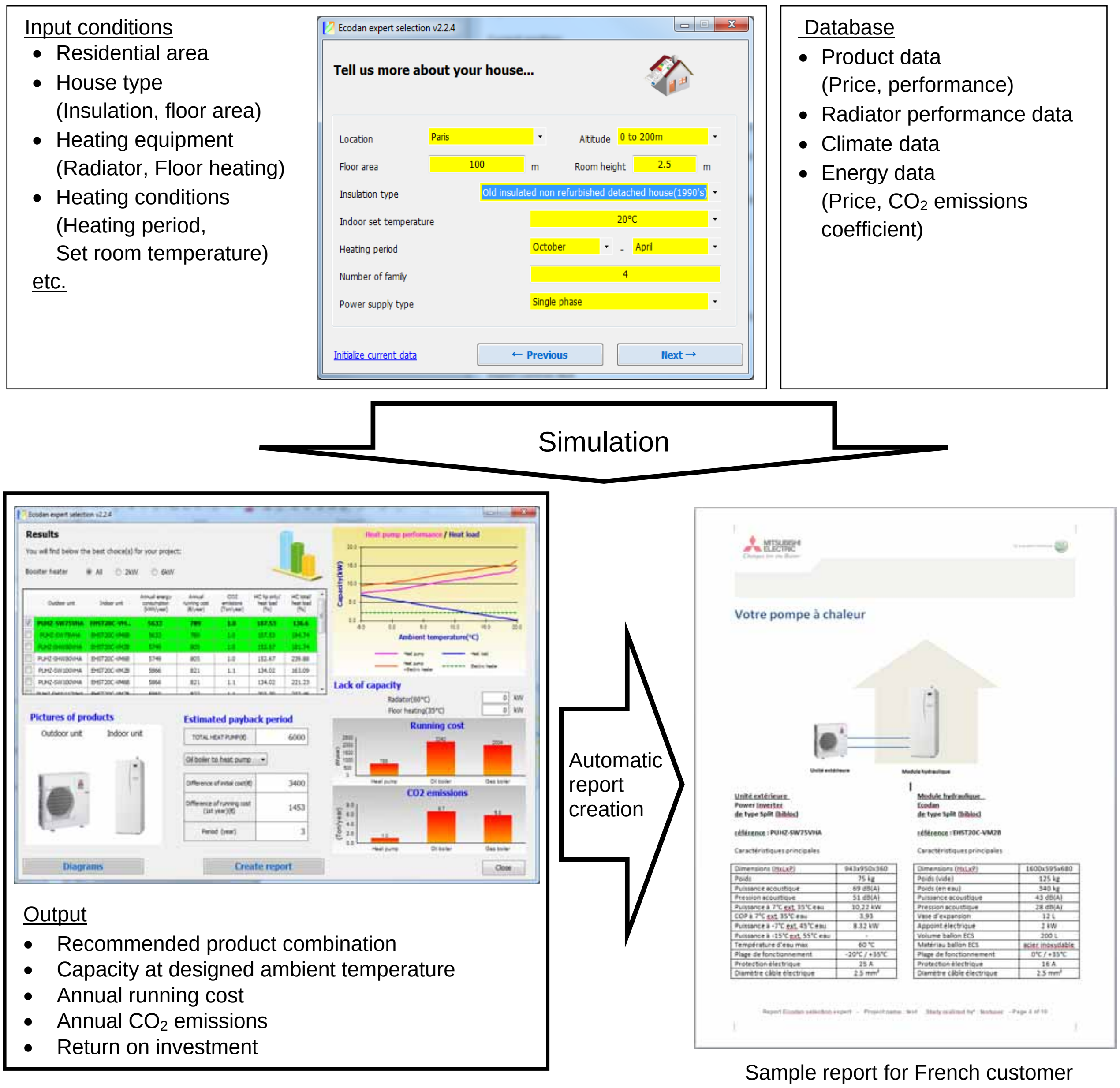

Fig. 5 Air to water energy simulation tool

energy saving performance compared with existing energy source (oil, gas and electrical boiler)
- Return on investment by installing ATW system

In addition, the tool can generate reports for the selected product combination automatically.

With these functions, the tool enables sales people to suggest a suitable product combination taking into consideration the various differences of country, residential area, house type, heating operation pattern, etc.

4. Evaluating GHG during product use

Mitsubishi Electric seeks to calculate GHG emissions throughout the Group's supply chain. The existing calculation method based on Scope 3 of the GHG protocol and ISO standard is only a calculation framework; it does not consider the effects of various differences dealt with by our tool. Since GHG emissions during product use account for a majority of total GHG emissions, such variations in conditions affect the overall GHG emissions. Therefore, we evaluated the variability of calculation results based on the following different calculation conditions.

- Area: warmer area to colder area in the same country
- Insulation performance: variations from –20% to +20%
- Heating period: 5 to 7 months
- Set room temperature: 19 to 21°C

Figure 6 shows the calculation results for different calculation conditions. Comparing the maximum and minimum values, there is a difference of up to about 30% even if only one calculation condition is changed. So if several calculation conditions differ in a single case, the difference between the maximum and minimum values may be much larger. Therefore, various conditions must be considered when calculating GHG emissions, and suitable combinations should be chosen from various conditions for benchmarking. These results were reported in the international conference on EcoBalance.(3)

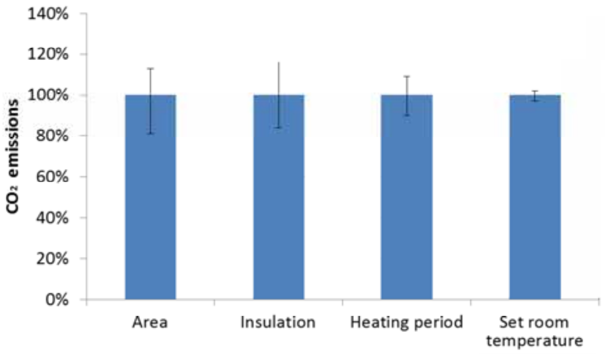

Fig. 6 Variation of CO_2 emissions based on different calculation conditions

5. Conclusion

This paper introduced an ATW energy simulation tool which can simulate annual energy consumption, running cost and CO_2 emissions taking into consideration the customer's various conditions such as residential area, house type, and heating operational conditions. This tool will help sales people to suggest a suitable product combination for a particular customer, to encourage the introduction of ATW. Mitsubishi Electric will thus help to reduce GHG emissions in Europe.

References

(1) Cargarrielea, Carlops, West Linton, Scottish Borders, Report on Energy Monitoring Results including Renewable Technologies (2012), 2013
(2) nZEB definitions in Europe, The REHVA European HVAC Journal, Volume 51, Issue 2, March 2014
(3) Chie Uchiyama, Estimating multiple changes of GHG emissions on Mitsubishi Electric Group's supply chain; category 11 – possible variation of GHG during use stage, Eco Balance 2014, October 2014
(4) http://www.bmwi.de/EN/Topics/Energy/Conventional-energy-sources/gas,did=690442.html, Federal Ministry for Economics Affairs and Technology, Germany, 2011
(5) Off-gas consumers – Information on households without mains gas heating, Consumer Focus, U.K., 2011
(6) Energy balance for France, SOeS (Service de l'observation et des statistiques), 2012

Material Sensing Technologies in Post-Consumer Electronics Recycling System

Authors: *Yasushi Uehara**and *Sonoko Umemura**

We have established a high-quality plastic recycling system that utilizes X-ray absorption phenomena, enables high-speed sorting of high-bromine-content resins from shredded mixed plastic flakes supplied from the recycling of electric home appliances, and recovers RoHS-compliant materials (RoHS: Restriction of Hazardous Substances directive pertaining to electrical and electronic equipment). Instead of a method that senses the bromine itself, we focused on the fact that a plastic flake containing highly brominated flame retardant absorbs more X-rays than a flake without such retardant, and established a method to determine whether or not bromine is present in a plastic flake based on the shade level of its X-ray image. By optimizing the conditions for X-ray irradiation and the detection of transmitted X-rays, as well as by controlling the air jet with high precision to remove unwanted materials, the new process has achieved a bromine concentration of less than 300 ppm and a yield percentage of more than 90% at a processing rate of 720 kg/h.

We have also developed an automated purity inspection system for the sorted and recycled plastic flakes. This system employs infrared light as the sensing probe because it is less sensitive to the flake color or additives. Infrared light is irradiated onto automatically conveyed plastic flakes, and the resin type-specific information carried in the reflected light is instantly analyzed to identify the resin type. The new system automatically identifies polypropylene (PP), polystyrene (PS) and acrylonitrile-butadiene-styrene (ABS) resins with an accuracy of over 99% in about one second, enabling automatic purity inspection.

1. Introduction

Mitsubishi Electric has been developing a wide range of technologies for closed-loop self-recycling of post-consumer electronics to help establish a recycling-based society. Among others, Mitsubishi has established a process for high-level sorting and recovery of high-quality raw materials from mixed plastic flakes obtained from shredded parts that are difficult to disassemble manually. Green Cycle Systems Corporation (GCS) employs these technologies to process about 10,000 tons of flakes every year and recover the raw materials, which are eventually reused for some of Mitsubishi Electric's products. The recycled plastic materials used for products must be of high purity because the presence of any impurities degrades the physical properties of the material. In addition, specific brominated flame retardants for plastics, which are thought to be hazardous, used to be applied in old home electric appliances, and thus bromine-containing plastic flakes must be eliminated from recovered plastic materials. Accordingly, the bromine must be instantly detected in the recycling process. We have therefore applied analysis-based material sensing to ensure that the recovered plastics are of high quality.

2. Material Sensing in Industrial Process

There are only a few known examples in industrial processes involving multiple kinds of materials where the flowing material itself is identified by material sensing: e.g., in some vacuum processing, whether or not a certain process is ready to start is determined by the sensing of residual gas components in the exhaust; and composition sensing in some petroleum refining processes by separating part of the intermediate product into a branch flow. However, these cases are considered sample tests, and 100% inspections are not performed. The sensing method adopted for the sample test is of a high-precision type and is based on the same principle as the individual material analysis.

However, such a method based on individual material analysis is not suitable for 100% inspections of high-volume products; instead, pass/fail is judged by acquiring two-dimensional signals and binarizing their intensity. For example, X-ray imaging is widely used for inspecting food and medicine to detect any foreign particles.

3. Material Sensing at the Plastic Recycling Site

3.1 Detection and elimination of bromine-containing resins for environmental compatibility

*Advanced Technology R&D Center

3.1.1 Bromine detection by X-ray imaging[1]

Recycled plastics used for electric home appliances must comply with the RoHS directive, and specific brominated flame retardants remaining in the recovered plastics must be eliminated. Essentially, it is sufficient to eliminate only those plastics that contain regulated substances. However, sorting out these specific substances requires a very sophisticated material analysis, which is not suitable for high-volume sorting. Therefore, we set the goal of removing all bromine-containing resins without detecting the bromine itself, and achieved a residual bromine concentration of less than 300 ppm in the recovered plastics. As described above, whether or not bromine is present is determined from the shade level of the X-ray image.

The majority of plastics used for electric home appliances are accounted for by three types: PP, PS and ABS. Their main constituent elements are carbon (C) and hydrogen (H), which are almost “transparent” to X-rays. In contrast, bromine is heavier than carbon or hydrogen and thus absorbs more X-rays. The value of X-ray transmittance can be calculated from each element’s known absorption coefficient. As an example, Fig. 1 shows the calculations for the X-ray transmittance of 1- and 5-mm-thick ABS ($C_{15}H_{17}N$) plastic plates, the heaviest plastic among the above three kinds; and 1-mm-thick dibromobiphenyl (DiBB, $C_{12}H_8Br_2$) plate, one of the brominated flame retardants. For the X-ray imaging of industrial materials, the X-ray source is often operated at a voltage of 50 kV or higher. However, Fig. 1 shows that the difference in transmittance is significant in the range of low X-ray energy, and the thickness dependence of the transmittance of ABS is relatively less significant than the absorption by the bromine contained in DiBB. Note that the actual concentration of bromine-based flame retardants in the plastics is only a few weight percent at the most, and thus the dependence of the X-ray transmittance on the flake thickness and bromine content must be accurately determined; otherwise, non-bromine-containing but thick plastic flakes might be removed, resulting in a low yield of recovered bromine-free resins.

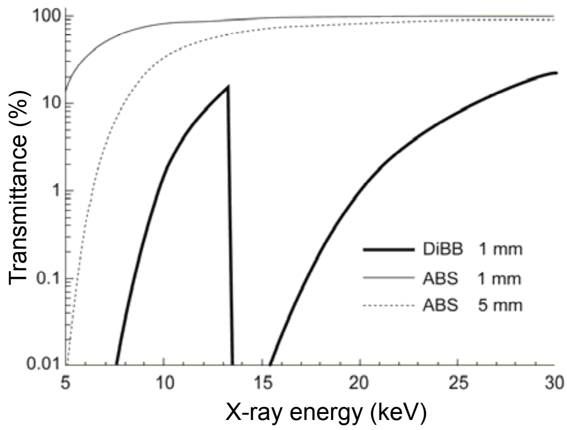

Fig. 1 X-ray transmittance of ABS plates and brominated flame retardant (DiBB).

3.1.2 Equipment for sorting bromine-containing resins[2]

Figure 2 illustrates schematically the commercial-scale sorting machine based on X-ray imaging, which is currently used for eliminating bromine-containing resins. Some of the measurements acquired by this equipment are also shown. Plastic flakes are supplied from the hopper and conveyed to the inspection stage at 100 m/min. Since the conveyer speed is fast enough compared to the feeding rate, the flakes are dispersed on the conveyer without overlapping each other and then they are thrown into the air from the end of the conveyor. Directly above the throwing point is the X-ray source; and directly below is a line sensor to measure the X-ray intensity transmitted through each flake. If the transmitted intensity is below the threshold level, the air gun located downstream from the sensor

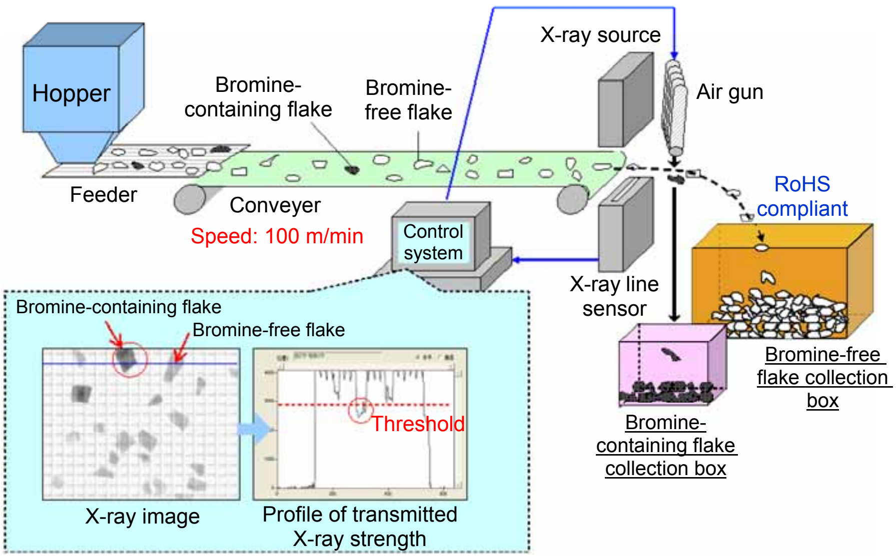

Fig. 2 Schematics of X-ray imaging based sorting machine for eliminating bromine-containing plastics

shoots the corresponding flake into the collection box located in line with the air gun; otherwise, the flake drops into the recovery box placed downstream. Each flake is thrown off the conveyer at an initial speed of about 2 m/s, and while the flake is in the air, it is inspected and sorted within milliseconds. The X-ray transmittance is dependent only on the thickness and bromine content of the flake without any influence from the conveyer material, resulting in high-precision detection and elimination of bromine-containing resins. As a result, the recycling runs at a processing rate of 720 kg/h, recovering plastic flakes with a bromine concentration far below the environmental regulation level of 300 ppm and with a yield percentage of 90% or higher.

3.2 Resin type identification for automated purity inspection

In addition to PP, PS and ABS resins, many different kinds of plastics are included in the shredded mixed plastic flakes. Therefore, it is impractical to achieve zero contamination in a large-scale recycling process, and so a purity inspection is performed for each lot on a sampling basis. Consequently, we have developed an automated inspection system.

3.2.1 Selection of identification probe

Noncontact and nondestructive probes known for resin identification include near-infrared light, mid-infrared light, and laser Raman spectroscopy. Among these, identification of resin type using reflected near-infrared light has proven to be effective for white resins; however, colored resins do not reflect near-infrared light and thus cannot be identified. Shredded mixed plastics recycled from electric home appliances contain a substantial amount of colored resins, and so near-infrared light cannot be used as the identification results should not be influenced by the resin color. Laser Raman spectroscopy can detect resin-specific signals in less than a second. However, our experiments have shown that it is difficult to identify white and colored resins under the same conditions because of the scattering of laser light and the fluorescent light from white specimens induced by the laser irradiation.[3] In contrast, mid-infrared light spectroscopy can identify all resin types under conditions relatively less susceptible to external disturbance, although it is less effective than laser Raman spectroscopy in terms of signal intensity and hence requires a longer evaluation time. Consequently, we have selected the reflection spectrum of mid-infrared light as the best probe for continuous, high-volume, and noncontact resin identification.

3.2.2 Identification algorithm

Figure 3 shows the infrared spectra (absorption) of PP, PS and ABS resins. The horizontal and vertical axes indicate the “wavenumber (unit: cm^{-1})” and the intensity of absorption, respectively. As described above, the main constituent elements are carbon (C) and hydrogen (H), and thus in each spectrum, absorption peaks attributable to the C-H bond appear at wavenumbers around 3000 cm^{-1}. It should be noted, however, that the profile of PP differs from that of PS and ABS, and the spectrum analysis in this range can distinguish PP from PS and ABS. While the spectrum analysis in this range cannot distinguish between PS and ABS because of their perfect resemblance, the spectrum of ABS exhibits a distinct absorption peak at 2350 cm^{-1} that is not included in the PS spectrum. Consequently, we have developed an algorithm to identify each unknown plastic flake – either PP, PS or ABS – based on the spectrum profile around 3000 cm^{-1} and the presence of absorption peaks at 2350 cm^{-1}. We have verified that all impurity plastics, except for acrylonitrile styrene (AS) that is similar to ABS, can be distinguished with this algorithm and separated from the three main plastics.

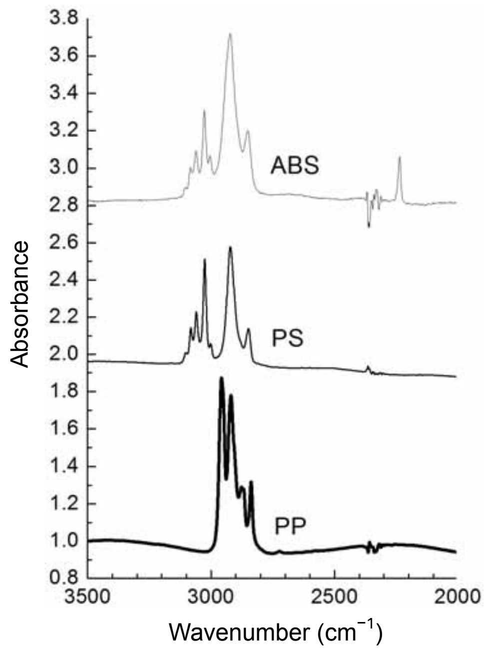

Fig. 3 Infrared absorption spectra of PP, PS and ABS resins

3.2.3 Improvement of identification speed and precision

Fourier transform infrared (FTIR) spectroscopy is considered to provide the fastest measurements of infrared (absorption) spectra with the highest resolution. In FTIR spectroscopy, continuous infrared light is directed from the light source to the interferometer, split into two beams having different optical path lengths, and then irradiated onto the specimen where either absorption or reflection of the light is measured. During the measurement, a mirror in the interferometer makes reciprocating movements, and in one cycle, the interfering light beams covering the target wavelength range are measured. The Fourier transformation of the obtained signals gives a spectrum that describes the relationship between the wavelength and the absorption (reflection) intensity. To increase the measurement speed, the mirror's reciprocating movements must be faster at a shorter distance. However, there is an upper speed limit, and a shorter distance reduces the wavelength resolution. Therefore, instead of pursuing both high sensitivity and high resolution, which are required for an ordinary material analysis, we designed the system specifically for high-speed identification of the three main plastic types. To this end, we determined the critical resolution that ensures the precision of the spectrum profile analysis in the vicinity of 3000 cm^{-1}, and limited the mirror's movement to the corresponding distance. Consequently, we have achieved high-precision identification at a high speed of less than one second per flake.

3.2.4 Resin type sorting machine

Figure 4 shows the configuration of the automated resin type sorting machine, which was jointly developed with Shimadzu Corporation. The conveyer disc has many holes and is arranged with an inclination so that a plastic flake is held by its own weight at each hole and is automatically conveyed to the identification position where the double beams from the mid-infrared Fourier spectrometer are focused and irradiated onto the specimen and the light reflected from the surface is measured. The resin type of each flake that passes through the spectrometer is identified according to the above-described algorithm, and type-identified plastic flakes are selectively collected using the air guns located at the lower side of the disc. This machine can identify and separate the three main plastics – PP, PS and ABS – with an accuracy exceeding 99%. The machine was used on a trial basis for the purity inspection of several lots of PP, PS and ABS materials recovered at GCS. The results showed good agreement with the conventional inspection for PP, PS, and ABS using chemical analysis, demonstrating the usefulness of the system for automated purity inspection.

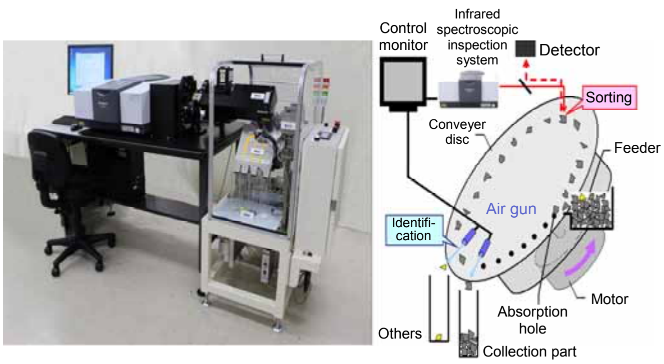

Fig. 4 Outline of automated resin sorting machine based on mid-infrared spectroscopy

It should be noted that Shimadzu Corporation has released a commercial version of the automated resin type sorting machine equipped with a spiral type flake conveyer plane disc.[4] This machine has been installed at the GCS facility for the purity inspection of recovered plastic flakes.

4. Conclusion

X-ray imaging based sorting is currently used to eliminate bromine-containing resins at GCS, where the successful production of environmentally compatible products has been achieved. Resin sorting technology based on mid-infrared spectroscopy is also applied to purity inspection, and further development is under way to expand its application for estimating the composition ratio of mixed plastic flakes prior to feeding them to the large-scale sorting process. At the electrostatic sorting stage in the large-scale sorting process, the state of the electrostatic charge varies depending on the composition ratio of mixed flakes, resulting in a variance in the sorting results. If a rough estimation of the composition ratio were available prior to the input to electrostatic sorting, the charging level and sorting conditions could be controlled and the yield percentage could be improved.

The development presented in this paper is the outcome of the FY2009 commissioned project sponsored by the Ministry of Economy, Trade and Industry, "Development of Advanced Plastic Analysis Technology," and the FY2011 subsidy for the development of practical applications of industrial technologies, "Advanced Plastic Identification Technology and Material Recycling Technology." Development of the optical identification technology was jointly conducted with Shimadzu Corporation.

References

(1) Mariko Mashimo, et al.: "Recycling Technology for RoHS Compliant Plastics", Mitsubishi Denki Giho, 83, No. 8, 473–476 (2009) (in Japanese)
(2) Akira Yamada, et al.: "Advanced Recycling Technologies for Plastics used in Home Appliances", Mitsubishi Denki Giho, 85, No. 12, 692–695 (2011) (in Japanese)
(3) Mitsubishi Electric Corporation: Project report on the FY2009 Commissioned Research and Development project sponsored by the Ministry of Economy, Trade and Industry (Development of Advanced Plastics Separation Technology) (in Japanese)
(4) Shimadzu Corporation: Press release (October 22, 2014)

Purification of Water Environment by High-Concentration Ozone

Authors: *Nozomu Yasunaga** and *Tokiko Yamauchi**

1. Introduction

Ozone water treatment utilizes the strong oxidizing power of ozone to decompose refractory organic substances in the water. In the field of water purification, ozone is used for advanced water purification to eliminate taste and odor substances and reduce the trihalomethane formation potential. Ozone treatment is also effective for disinfection and decolorization, and thus is applicable to the improvement of water quality of treated sewage effluent, providing an effective means for water environment purification and wastewater reuse. However, there are concerns about the high cost and bromate formation as a byproduct of the ozone treatment. To widen the application of ozone water treatment in water supply and water sewage and maintain a healthy water environment, it is necessary to improve the quality of treated water and reduce the cost.

The recently improved efficiency of the ozone generator and increased ozone concentration have helped to reduce the size and cost of the ozone treatment system.(1) Mitsubishi Electric's ozone generator is of a silent discharge type, which generates ozone by feeding oxygen or air into the discharge space where an alternating high voltage is applied. The structure of the ozone generator and discharge tube is illustrated in Fig. 1. Inside the tank, the appropriate number of discharge tubes is installed to provide the predetermined ozone generation capacity by increasing/decreasing the number of tubes. Inside each glass tube, one end of which is closed, a metal conducting layer is formed to serve as a high-voltage electrode. The glass tube is inserted so that a uniform gap from the earth electrode is ensured, and the heat generated by the electric discharge is cooled down by the circulating water outside the earth electrode.

As depicted in Fig. 2, the diameter of the electrode is reduced to a quarter of the previous size. With this design modification, while the surface area per electrode is reduced to a quarter, the number of electrodes that can be inserted into the same tank is sixteen times greater than before, and thus the total surface area of electrodes becomes four times as compared with the previous design. Since the ozone generation rate is proportional to the surface area of the electrodes, the cross-sectional area of the tank with the same generation rate can be reduced to a quarter, or the diameter of the tank can be halved. In addition, the reduced interelectrode gap improves the cooling efficiency and thus provides more highly efficient generation of ozone, which easily decomposes at a high temperature. Furthermore, the discharged electric power density can also be increased, contributing to the downsizing of the ozone generator.

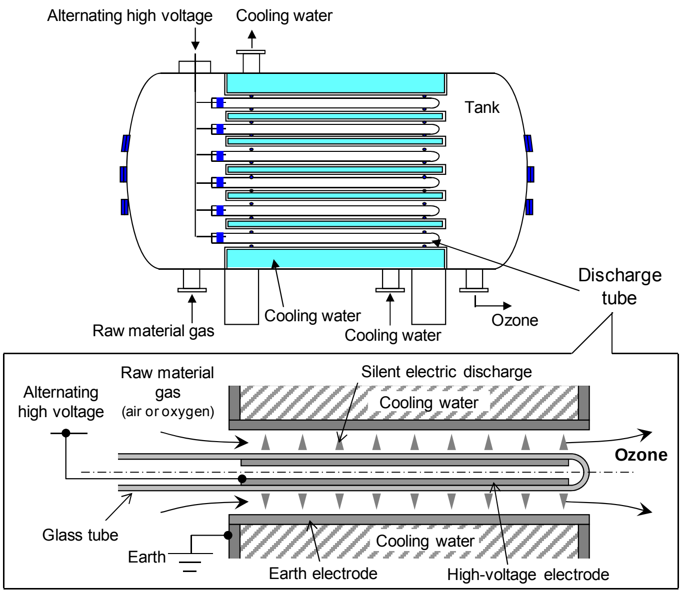

Fig. 1 Structure of ozone generator and discharge tube

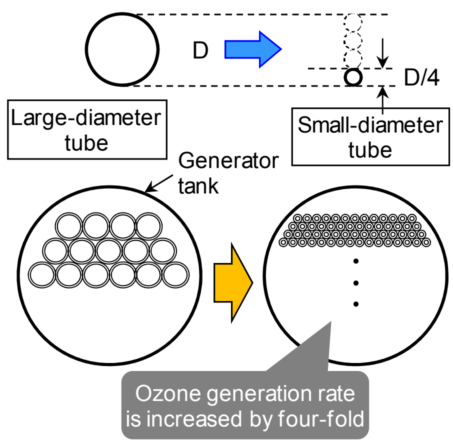

Fig. 2 Downsizing of tank by reducing discharge tube diameter

*Advanced Technology R&D Center

The reduced interelectrode gap also enables the electric field intensity to be increased, thus efficiently producing a higher concentration of ozone. Mitsubishi Electric has reduced the interelectrode gap to less than one fifth that of the conventional design by means of high-precision electrode fabrication and accurate gap supporting technology. Consequently, we have achieved the industry's highest ozone gas concentration of 240 g/Nm^3.

These advanced ozone generation technologies have improved the performance of water treatment using high-concentration ozone by providing higher ozone transfer efficiency and faster decomposition of organic substances.[2] However, much remains unknown regarding the formation of bromate and other byproducts, which are suspected to be hazardous to human health.

This paper describes the characteristics of ozone transfer efficiency, bromate formation and decomposition of organic substances evaluated with varying ozone gas concentrations.

2. Methodology and conditions of experiment

2.1 Experimental conditions

Figure 3 is a schematic diagram of the experimental apparatus and Table 1 shows the experimental conditions.

Experimental untreated water was prepared by adding a predetermined amount of potassium bromide

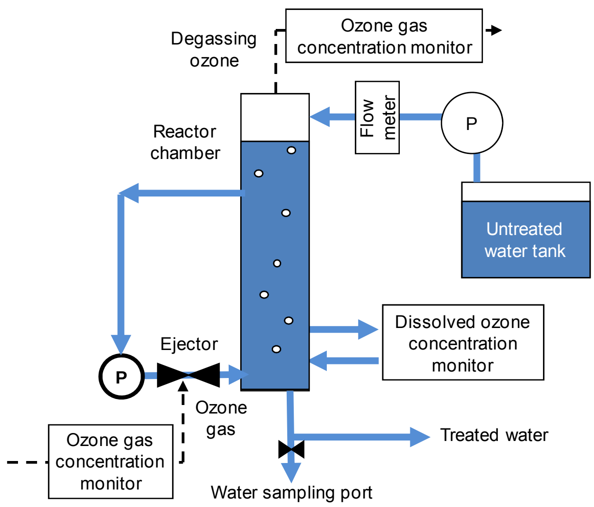

Fig. 3 Schematic diagram of experimental apparatus

(KBr) to unchlorinated industrial water, which was sedimentation-treated surface water from the Yodo River water source. The continuous water treatment reactor is of a counter-flow type with an inner diameter of 50 mm and an effective capacity of 2.95 L; and a circulation flow path is provided in the reactor so that complete mixing conditions are established in the flow inside the reactor, regardless of the flow rate of the ozone gas. The untreated water was fed to the reactor at a flow rate of 0.59 L/min and the retention time was set to 5 min. Meanwhile, ozone gas was generated using oxygen as the raw material and added to the untreated water at concentrations of 20, 50, 150 and 210 g/Nm^3. Ozone gas at a predetermined flow rate was injected into the untreated water using an ejector arranged in the circulation path. After starting the injection of ozone gas, we waited for at least 30 min until the degassing ozone concentration and the dissolved ozone concentration reached steady states, and then we took treated water samples for the water quality analysis. The main analysis items were the absorbance at a wavelength of 254 nm which are among the organic substance indicators (UV254) and the concentration of bromate and bromide ions (BrO_3^- and Br^-, respectively).

3. Experimental results and discussion

3.1 Ozone related indicators

Figures 4 and 5 show the variation in ozone transfer efficiency with respect to the ozone gas concentration and the gas-to-liquid ratio (G/L), respectively. As shown in Fig. 4, at an ozone dose of 10 mg/L, the higher the ozone gas concentration, the higher the ozone transfer efficiency. In contrast, as shown in Fig. 5, the lower the gas-to-liquid ratio, the higher the ozone transfer efficiency, regardless of the ozone gas concentration. These results suggest that at the same ozone dose, a higher ozone gas concentration gives a lower G/L and hence a higher ozone transfer efficiency.

These results show that the higher the ozone gas concentration is, the more effectively ozone can be utilized.

Figure 6 shows the variation in the amount of ozone dissolved and consumed with respect to the ozone gas concentration when the amount of ozone transferred was 4 mg/L. The amount of ozone

Table 1 Experimental conditions

Item	Super high concentration	High concentration	Intermediate concentration	Low concentration
Ozone gas concentration (g/Nm^3)	210	150	50	20
Ozone gas flow rate (mL/min)	13-42	18-60	40-360	60-450
Ozone dose (mg/L)	0.02-0.07	0.03-0.10	0.07-0.60	0.10-0.76
G/L (−)	4.4-14	4.5-15	3.3-30	2.1-14
Temperature (°C) and pH (−)of untreated water	20-22, 7.3-7.5			
Br^- concentration of untreated water (μg/L)	192-194			

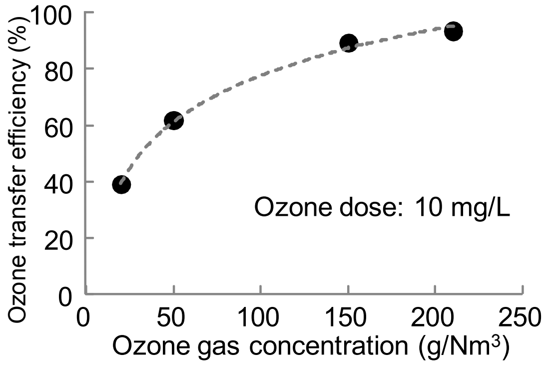

Fig. 4 Variation in ozone transfer efficiency vs. ozone gas concentration

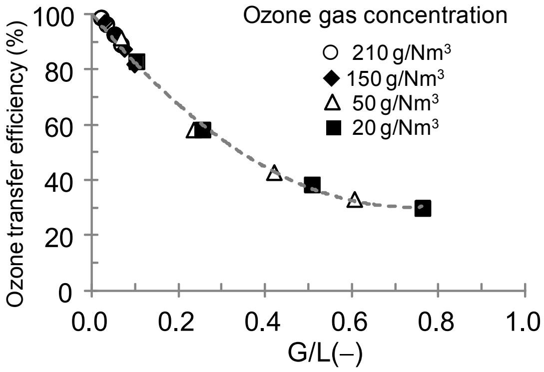

Fig. 5 Variation in ozone transfer efficiency vs. G/L

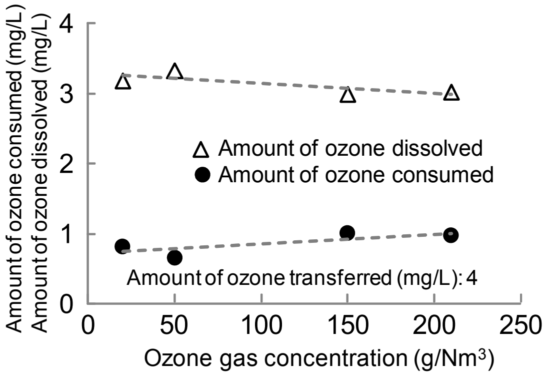

Fig. 6 Variation in amount of ozone consumed and dissolved vs. ozone gas concentration

consumed was calculated by subtracting the concentration of dissolved ozone from the amount of ozone transferred in one liter of treated water (ozone consumed = ozone transferred − concentration of dissolved ozone). This chart shows that as the ozone gas concentration increases, the concentration of dissolved ozone decreases and the amount of ozone consumed increases, a tendency that is contrary to Henry's law. Since ozone is a very unstable substance, it self-decomposes and finally becomes oxygen while generating OH radicals. We thus infer that the higher ozone gas concentration accelerates the generation of OH radicals due to ozone self-decomposition, which in turn increases the amount of ozone consumed, resulting in a decrease in the concentration of dissolved ozone.

3.2 Characteristics of bromate formation and organic substance decomposition

Figure 7 shows the variation in the amount of bromate formed and the concentration of bromide ions (Br^-) with respect to the ozone gas concentration when the amount of ozone transferred was 4 mg/L. Bromate is formed when Br^- is oxidized by ozone, via the creation of hypobromous ions and other intermediates. The amount of bromate formed tended to increase with the increase in the concentration of dissolved ozone. The chart shows that the higher the ozone gas concentration, the smaller the amount of bromate formed. We infer that this tendency is attributed, as shown in Fig. 6, to the reduction in the concentration of dissolved ozone as a result of an increased amount of ozone consumed with the increase in the ozone gas concentration, while the ozone consumed does not contribute to the bromate formation. In addition, the higher the ozone gas concentration, the higher the Br^- concentration in the treated water. Experiments using a pure water system have also shown the tendency of an increase in the Br^- concentration and a decrease in the amount of bromate intermediates.(3) Consequently, we infer that in our experiments as well, a decrease in the amount of intermediates for bromate formation caused the decrease in the amount of bromate.

Figure 8 shows the variation in the residual UV254 rate with respect to the amount of ozone transferred. UV254 is an indicator of the amount of ozone-reactive organic substances, and it is considered that the higher the UV254, the higher the organic substance concentration. The residual UV254 rate is defined as the ratio of UV254 in treated water to that in untreated water. As shown in this chart, the residual UV254 rate sharply decreased to 60% at an transferred ozone amount of 2 mg/L; and then as the amount increased from 2 to 13 mg/L, the rate gradually decreased to 44%. We infer that the organic substances likely to react with ozone were decomposed by the time the amount of transferred ozone reached 2 mg/L; then above this transfer level, other organic substances less likely to react were slowly decomposed. In contrast, when the residual UV254 rate of the treated water decreased, the concentration of total organic carbon (TOC) showed no variation (chart is not shown), and thus we infer that the conversion to inorganic substance did not take place. In addition, there was a variance in the residual UV254 rate, and no dependence on the ozone gas concentration was observed. We infer that despite a small variance in the UV254 of untreated water, the reactivity with ozone varies from organic substance to substance, resulting in the variance.

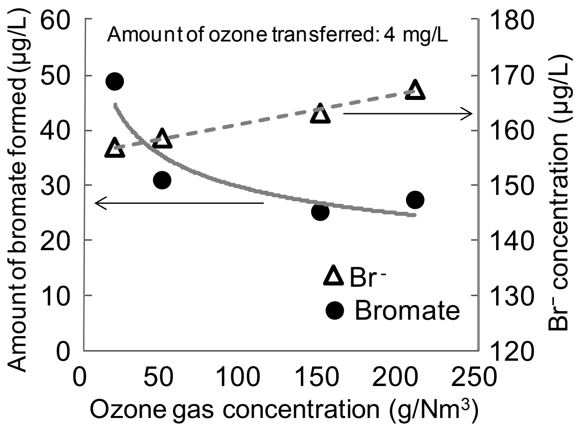

Fig. 7 Variation in the amount of bromate formed and the Br^- concentration vs. ozone gas concentration

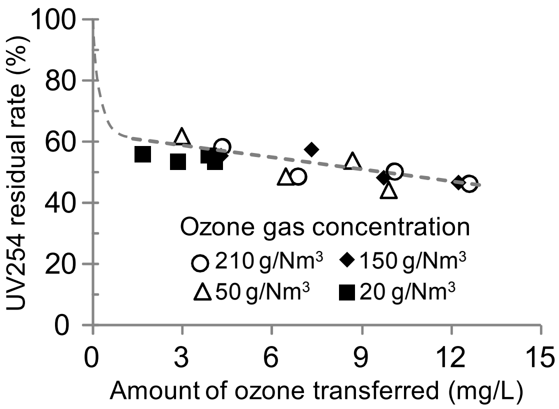

Fig. 8 Variation in residual UV254 rate vs. amount of ozone transferred

4. Conclusion

The following summarizes our experimental study on the application of high-concentration ozone gas to water treatment:

At the same ozone dose, the higher the ozone gas concentration, the lower the gas-to-liquid ratio (G/L) and hence the higher the ozone transfer efficiency. Therefore, the higher the ozone gas concentration, the more effectively ozone can be utilized.

The higher the ozone gas concentration, the smaller the amount of bromate formed in contrast to the amount of ozone transferred. We infer that as the ozone gas concentration was increased, the amount of ozone consumed increased and thus the concentration of dissolved ozone decreased, while the ozone consumed did not contribute to the bromate formation.

The decomposition of UV254 substances was almost independent of the ozone gas concentration. No dependence on the ozone gas concentration was observed in the performance of eliminating organic substances.

The phenomena underlying these results are academically interesting, as well. We will continue to analyze the effects of high-concentration ozone on water treatment by means of numerical simulation using a radical reaction model that includes ozone. The method described in this paper provides a promising measure for solving the increasingly serious problem of water shortages. We will continue to develop water treatment technologies that use ozone more effectively to contribute to the purification of the global water environment.

References

(1) Masahiro Chikaishi, et al.: "Characteristics of ozone generation using noble metal catalyst," Proceedings of the 21st Japan Ozone Association Annual Conference, 56–60 (2012) (in Japanese)

(2) J. Hart, I. Walker and D.C. Armstrong: "The Use of High Concentration Ozone for Water Treatment," Ozone Science and Engineering, Vol. 17, 485–497 (1995)

(3) Nozomu Yasunaga, et al.: "Characteristics of ozone water treatment using high concentration ozone – Verification of the effect of suppressing bromate formation," Proceedings of Research Presentations, FY2013 National Conference (Japan Water Works Association), 140–141 (2013) (in Japanese)